Sustainable Energy Technologies and Assessments 77 (2025) 104323

Contents lists available at ScienceDirect

Sustainable Energy Technologies and Assessments

journal homepage: www.elsevier.com/locate/seta

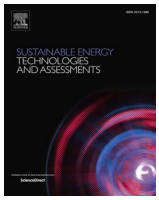

The impact of metal type on the pyrolysis product distribution of sugar beet pulp: An analytical Py-GC/MS study with alumina-based catalysts

Nurgül Özbay [a], Adife Şeyda Yargıç [a,*], Aydan Tatman [a], Fatma Eroğlu [b]

[a] Chemical Engineering Department, Engineering Faculty, Gulumbe Campus, Bilecik Seyh Edebali University, 11100 Bilecik, Türkiye
[b] Department of Chemistry, Faculty of Science, Ankara University, 06100 Ankara, Türkiye

ARTICLE INFO

Keywords:
Biomass
Catalytic pyrolysis
Me/Al_2O_3
Py-GC/MS

ABSTRACT

The bio-oil produced by non-catalytic pyrolysis of biomass is typically corrosive and unstable due to the presence of several reactive components. Either in-situ or ex-situ catalytic models can be utilized with appropriate catalysts to achieve selective distribution of pyrolytic products during the catalytic pyrolysis of biomass, resulting in the generation of high-grade bio-oil. This study investigated the catalytic performances of different metal-incorporated alumina-based catalysts concerning the product composition in the pyrolysis of sugar beet pulp at 550 °C in a pyrolysis–gas chromatography/mass spectrometry (Py-GC/MS) system. Nitrogen adsorption, Fourier transform infrared spectroscopy (FTIR), x-ray diffraction (XRD), and scanning electron microscopy (SEM) techniques were used to characterize the metal-loaded alumina catalysts. FTIR analysis of catalysts with angular morphology proved the existence of alumina and metal–oxygen bonds (Me-O, Al-O, and Me-O-Al) in the structures, and x-ray diffraction patterns confirmed that crystalline phases were formed. It can be said that the crystal structures and functional groups determined by XRD and FTIR analyses had significant effects on the catalytic pyrolysis activity and product distribution. The main organic compounds obtained from the non-catalytic pyrolysis of sugar beet pulp were acids. In addition to acids, ketones, and aldehydes are among the undesirable compounds. As a result of catalytic pyrolysis, the lowest amount of aldehydes was generated when Ni-loaded alumina catalyst was employed. Notably, catalytic performances of Ni/Al_2O_3 and Co/Al_2O_3 resulted in the highest yields of valuable compounds in terms of hydrocarbons. The amount of undesired acidic compounds among the products, which increase the corrosive effect, was reduced by ~51 % compared to the non-catalytic pyrolysis result with the employment of the Fe/Al_2O_3 catalyst.

Introduction

Given the coercing of energy and environmental sustainability, utilizing renewable resources such as biomass to produce hydrocarbon-based fuels and valuable chemicals has noteworthy application potential and wide consumer expectations. In recent years, pyrolysis has attracted intense interest in producing liquid fuels from biomass. However, the complicated biomass pyrolysis process, low calorific value, considerable oxygen content, and bio-oil's acidity restrict its utilization as a liquid fuel and chemical [1]. As a result, bio-oil needs to have its quality raised. Because of this, catalysts are frequently used throughout the biomass pyrolysis process to generate the required components, such as high-quality liquid fuels and chemicals with superior value [2].

Two classifications of catalytic pyrolysis exist: in-situ and ex-situ. Various studies have examined the performance of catalytic pyrolysis to manufacture hydrocarbon-based diesel or gasoline compounds and reduced oxygenating species in bio-oil. In the in-situ pyrolysis process, catalyst and raw material are provided simultaneously, while the solid and vapor phases' upgrading takes place in a reactor. In contrast, the ex-situ method involves the independent installation of feedstock and catalyst, hence, solid and vapor phases are produced in a reactor and a catalyst bed, respectively [3]. The biomass feedstock, catalyst nature, and operating parameters (i.e. temperature, biomass-to-catalyst (B:C) ratio, reactor kind, size of biomass particles, heating rate, and retention time) all affect the yields and characteristics of the bio-oil produced by catalytic pyrolysis [4–7].

The use of catalysts increases the yield of bio-oil yield and the amount of aromatic hydrocarbons. Production steps of aromatic hydrocarbons from lignocellulosic biomass are classified as follows: *i)* anhydrous sugars and furan substances produced from the

* Corresponding author.
E-mail address: seyda.guler@bilecik.edu.tr (A.Ş. Yargıç).

https://doi.org/10.1016/j.seta.2025.104323
Received 26 June 2024; Received in revised form 19 February 2025; Accepted 13 April 2025
Available online 19 April 2025

decomposition of cellulose and hemicellulose are the main starting pyrolysis products, *ii)* acid-catalyzed cellulose dehydration results in the formation of anhydrous sugar, which is subsequently followed by the dehydration generation of furanic compounds like methylfuran, furfural, small aldehydes, and water gas phase, *iii)* the catalyst and furan compounds undergo dehydration, oligomerization, decarbonylation, and decarboxylation reactions, which result in the production of a hydrocarbon pool and carbon monoxide [8]. Various kinds of catalysts, including molecular sieves, alkali metals, transition metals, and alkaline earth metals, have been studied to maximize the performance and efficiency of bio-oil and value-added chemical substances. Among these, certain metals and their oxides have demonstrated unique properties [9]. In that, transition metals like iron, cobalt, and nickel have been properly used for converting biomass into beneficial products.

Different catalysts or catalytic systems can facilitate specific reactions to produce desired compounds. It is important to note that most research utilizes just one type of efficient metal or an efficient metal supported on an alternate kind of porous support (such as γ-Al_2O_3). Corners and edges of the alumina have the greatest number of active surface sites, while sites on surface plates are probably not as reactive because of the absence of oxide structure. The loaded groups over the gappy sites would interact first while they also contain less reactive points at higher coverage. There is a severe lack of research on effective metals and identifying the relationship between them [10]. Metal-loaded alumina catalysts are a class of heterogeneous catalysts that consist of a porous alumina support material impregnated with metal ions or metal nanoparticles. The metal can be selected based on its catalytic properties and can include noble metals such as platinum, palladium, or gold, or base metals such as nickel, cobalt, or iron. The alumina support provides a high surface area and thermal stability, which can help to maintain the stability and activity of the metal catalyst. The metal ions or nanoparticles are distributed across the surface of the support material, providing an active site for catalytic reactions. Metal-loaded alumina catalysts can be employed in a variety of catalytic uses, including the generation of chemicals, petrochemicals, and fuels. Additionally, they can be used in environmental tasks like wastewater treatment or the removal of pollutants from the air. The performance of metal-loaded alumina catalysts can be affected by several variables, such as the metal loading, the preparation method, and the operating conditions. The choice of metal and preparation method can be optimized to achieve the desired catalytic properties for a given application.

Through the more environmentally friendly manufacturing of bio-oil and high-value chemical compounds, agricultural waste can be used as a renewable energy source that doesn't interfere with the generation of food. The pulp from sugar beets is one of the many forms of waste from agricultural operations. Turkey holds a significant position among the countries that produce beet sugar, it is ranked fifth globally, behind the United States, Russia, France, and Germany, and fourth on the European Continent after Russia, Germany, and France. The only utilizes for sugar beet pulp are as feed for animals and as a raw component for the paper and cosmetics sectors [11]. Moreover, it can serve as a feedstock for processes involving catalytic pyrolysis.

The immediate technique of pyrolysis–gas chromatography/mass spectrometry (Py-GC/MS) has been established to investigate the biomasses' pyrolytic behavior and characterize their volatile derivatives. Since it can detect all pyrolytic compounds more effectively than GC/MS of condensable materials (liquid fractions), which requires full condensation to identify under various operating circumstances, it has attracted a great deal of interest recently [12]. The present study aimed to prepare metal-alumina composite catalysts with active sites when employed in the catalytic pyrolysis process. In this direction, the Me/Al_2O_3 catalysts were produced by loading transition or alkaline earth metals, known to have favorable effects on bio-oil yield and quality, onto alumina support with high thermal stability. For the first time in the literature, the comparison of the effects of Me/Al_2O_3 catalysts on the pyrolysis product distribution obtained via catalytic pyrolysis of sugar beet pulp in the Py-GC/MS system constituted the original aspect of this study. This work was divided into two main areas: (i) synthesizing metal functionalized alumina catalysts (Me/Al_2O_3, Me: Ca, Mn, Fe, Co, Ni, and Zn) by the process of co-precipitation and characterizing them employing analytical methods like SEM, BET, and XRD; (ii) utilizing a Py-GC/MS technique to examine the catalytic performances of Me/Al_2O_3 catalysts in the sugar beet pulp pyrolysis to produce high-value-added bio-oil or chemicals.

Materials and methods

This section included the procedures for preparing biomass, synthesizing catalysts, and characterizing them to ascertain their characteristics. Py-GC/MS studies were also provided comprehensively.

Raw material

The sugar factory in the vicinity of Eskişehir, Turkey's Central Anatolia Region, provided the sugar beet pulp (*SBP*) for this study. Pulp materials were initially milled to get mean particle size. Prior to the pyrolysis experiments, *SBP* was dried at 105 °C for 16 h and stored in a desiccator; hence, all pyrolysis data was recorded on a dry feed basis. The weight fractions of moisture, fixed carbon, ash, and volatile matter in *SBP* were determined via proximate analysis. The elemental analyzer (Leco CNH628 S628) was employed for the ultimate analysis, then Dulong's Formula (1) was applied to compute the feedstock's higher heating value (HHV) based on the elemental analysis results [13]:

$$HHV(MJ/kg) = 33.83C + 144.3(H - O/8) + 9.42S \quad (1)$$

Sugar beet pulp was examined using the ATR method in a Fourier transform infrared spectroscope (FTIR, Perkin Elmer Spectrum 100) to discover structural groups in the 4000–400 cm^{-1} wavelength region. Utilizing a Setaram Labsys Evo thermogravimetric analyzer (TGA) in a nitrogen atmosphere, the thermal stability of *SBP* was evaluated. 10 mg of *SBP* was used for the TG analysis, which ran from ambient temperature to 900 °C. The *SBP*'s morphology was investigated by a scanning electron microscope (Zeiss Supra VP 40).

Catalysts Synthesis and Characterization

Micro/mesoporous catalysts developed by loading various metals onto support materials at different ratios (1–20 % by weight) are utilized in catalytic pyrolysis. The pyrolysis of beech wood using ZSM-5 modified with Ni and Co at metal loadings ranging from 1 to 10 wt% [14], of coconut oil with 1 to 5 wt% Ni-incorporated SBA-15 [15], of cellulose with 5 % Ni-doped γ-Al_2O_3, SBA-15 or mesostructured cellular foam (MCF) silica [16], and of Yunnan pine with ZSM-5 containing 1, 5, and 10 wt% Zn, Ga, Ni, Co, Mg, or Cu [17] were among the studies implementing the metal-incorporated catalysts. The objective of this study was to examine the impacts of various metal types on the catalytic pyrolysis products of sugar beet pulp at a single metal loading level of 5 wt % concerning the existing literature as a guide. The co-precipitation technique was utilized to synthesize 5 wt% of various metal-containing Me/Al_2O_3 catalysts (Me: Ca, Mn, Fe, Co, Ni, and Zn). The detailed preparation procedure was available in our previous studies [13,18,19]. The co-precipitated catalysts underwent complete washing, filtration, and oven drying for 12 h at 110 °C. Then, the catalysts were calcined for 6 h at 900 °C in an air-flowed tube furnace.

To ascertain the crystal structure, x-ray diffraction (XRD) analysis was conducted using a PANalytical Empyrean diffractometer operating at 45 kV and 40 mA, and utilizing CuKaα radiation with λ = 0.15405 nm. With a counting time of two seconds for each step, the XRD patterns formed every 0.02° (2θ) in the range of 2θ = 10°–90°. N_2 adsorption/desorption tests were performed at −196 °C utilizing an automatic volumetric sorption analyzer (Micromeritics, ASAP 2020) to determine surface area, pore volume, and pore size. Previously, the

samples were degassed at 360 °C for 300 min. Applying the Brunauer-Emmett-Teller (BET) method, the surface areas of the catalysts were determined from N_2 adsorption/desorption isotherms. A Zeiss Supra VP40 scanning electron microscope was used to get images of the catalysts. Utilizing a Quorum Q150RESDC Sputter Coater, samples were fixed on carbon bands and coated with a platinum-thin layer in the presence of argon. A Perkin Elmer Spectrum 100 was implemented to analyze the catalysts using Fourier transform infrared spectroscopy (FTIR), which allowed for the identification of structural groups in the 4000–400 cm^{-1} wavelength region.

Py-GC/MS experiments

Biomass pyrolysis processes have been conducted in the literature at temperatures ranging from 300 to 700 °C. 550 °C was typically reported as the temperature at which the pyrolysis liquid product bio-oil generated with the highest yields; therefore, Py-GC/MS experiments were performed at this temperature in light of the reviewed studies. Sawdust pellets consist of Tectona grandis and Dalbergia [20], coffee grounds [21], pine sawdust [22], rice husks [23,24], tobacco residue [25], soybean cake [26], grape bagasse [27], pistachio shell [28], and cotton seed [29,30] were among the research subjects that chose 550 °C as the optimum temperature for the catalytic or non-catalytic pyrolysis processes. Experiments on sugar beet pulp pyrolysis took place via a Py-GC/MS system (Shimadzu QP2010-GC/MS, Frontier Py-2020-pyrolyzer). A tiny crucible containing around 1.0 mg of sample was filled and moved to the microfurnace at 550 °C. The system was sampled with only *SBP* for non-catalytic pyrolysis or a *SBP* + catalyst mixture with 10 wt% catalyst for catalytic pyrolysis. The Py-GC/MS system is categorized as a microreactor because only a small sample dose was adapted. When the studies conducted with the Py-GC/MS system were reviewed, it was seen that the biomass:catalyst ratio can be applied as 1:0.1 and 1:0.25 [31], 1:1 [32–35], 1:0.5, 1:1.5, and 1:2 [33], 1:5 and 1:10 [34]. In the thermochemical conversion processes in the Heinze type and tubular pyrolysis reactors that the research group has previously conducted, catalysts were generally added at 5–10 % by weight. In order to be parallel to these studies, since the sample proportion used in the reactor was less, it was preferred that 10 % by weight be added as the catalyst ratio. Ten minutes passed during the isothermal flash pyrolysis process at 550 °C for volatilization reactions. The reaction time used in the Py-GC/MS system is in accordance with many studies in the literature [31,36], and this time should be used for isothermal flash pyrolysis. Immediately after the biomass is decomposed into smaller molecules, a slight part of the volatile compounds is injected into a GC. The temperature of the injection section was 320 °C. Helium with ultra-high purity grade of 99.999 % flowed as the carrier gas at a rate of 1.0 mL/min. Pyrolysis products were separated chromatically with a Frontier Ultra Alloy column (30 m × 0.25 mm × 0.25 μm film thickness) set at 40 °C. The temperature of the GC oven was raised from 40 to 200 °C at a heating rate of 5 °C/min. This temperature was maintained for two minutes. The temperature was then raised to 300 °C at a heating rate of 20 °C/min and kept there for 11 min. The electron ionization (EI) mode was used to obtain mass spectra in the 20–500 *m/z* range at 70 eV [31].

Results and Discussion

Characteristics of biomass sample

Ultimate and proximate analyses

The proximate and ultimate analyses results of sugar beet pulp were given in Table 1. As seen, the ultimate analysis approved that sugar beet pulp contained higher volatile matter (74.5 %). Throughout the pyrolysis process, greater amounts of volatile matter are typically exposed to more liquid and gaseous fuel; the existence of volatiles also determines the potential for biomass combustion. The pyrolytic liquid yield and the higher heating value (HHV) are both more impacted by the quantity of extractives. Utilizing ethanol and toluene mixture as a solvent in a Soxhlet apparatus, the extractive content of the sugar beet pulp was ascertained as 10.58 %. The elemental analysis revealed that the sugar beet pulp's combined C, H, and O values were approximately 98.65 wt %, and the calorific value of raw material was determined to be 14.54 MJ/kg.

Table 1
Proximate and ultimate analyses results of *SBP*.

Proximate Analysis (wt%) Preliminary analysis	wt% ± SD(%)
Moisture	9.9 ± 0.14
Ash	4.2 ± 0.09
Volatile matter	74.5 ± 0.04
Fixed carbon[a]	11.4 ± 0.29
Structural analysis	***wt% ± SD(%)***
Extractive material	10.58 ± 0.33
Holocellulose	43.21 ± 1.83
Cellulose[b]	24.51 ± 0.28
Hemicellulose	18.70 ± 1.54
Lignin	24.34 ± 0.82
Ultimate Analysis (wt%)	
C	41.28
H	6.73
N	1.35
O[c]	50.64
HHV (MJ/kg)	14.54

[a] Calculated from difference. Fixed Carbon = 100 − (Volatile Matter + Ash + Moisture).
[b] Calculated from difference. Cellulose = Holocellulose – Hemicellulose.
[c] Calculated from difference. O = 100 – (C + H + N).

FTIR spectrum of SBP

The sugar beet pulp's chemical structure was revealed by the FTIR spectroscopy in the following ways. Fig. S1 (in Supplementary Information) displayed the presence of various atomic groups and structures (–OH, $–CH_2$, C=O, C-O-C, and so on) in sugar beet pulp. The location and shape of the band 3333 cm^{-1} were consistent with the hydroxyl groups' participation in hydrogen bonding. In any other case, the band ought to be sharper and situated at significantly greater wavenumbers [37]. Bands representing free –OH groups were observed at ~ 3625 cm^{-1} for alcohols. There was a broadening tendency for phenols and carboxylic acids towards lower wavenumbers 3605 cm^{-1} and 3530 cm^{-1}, respectively [38]. The υ_{as} and υ_s vibration modes of the methyl and methylene groups were linked to the band at 2922 cm^{-1}. Utilized in methyl group evaluation, the distinctive absorption of the methyl group around 1377 cm^{-1} served a diagnostic purpose. Furthermore, the relative abundances of the CH_2 and CH_3 groups were indicated in the 1400 cm^{-1} band. The band near 1460 cm^{-1} was often stronger than at 1377 cm^{-1} for organic substances. Bands at lower frequencies were produced by the CH_2 groups' secondary bending vibration modes, such as twisting, wagging, and rocking. These bands were rarely beneficial since they were typically weak [39]. Sugar beet pulp's spectra showed a shoulder at 1626 cm^{-1} that could be attributed to υ(C=C) vibrations in terminal olefinic C=C bonds. The absorption maxima may move toward lower wavenumbers due to band overlapping in the spectral region between 1700 and 1600 cm^{-1}. There were just two easily discernible aromatic skeletal stretching bands in the spectrum, at 1515 and 1460 cm^{-1}. As is typical for aromatic rings, the band at 1515 cm^{-1} was stronger than at 1595 cm^{-1}. The CH_3 and CH_2 bands overlapped with the peak at 1460 cm^{-1} [40]. Two neighboring hydrogen atoms in *p*-disubstituted phenyl groups were represented by an individual band at 779 cm^{-1} [38].

Thermal analysis

The thermogravimetric (TG) and derivative thermogravimetric (DTG) profiles of sugar beet pulp, which was heated at a rate of 10 °C per minute from ambient temperature to 900 °C, were displayed in Fig. S2. In general, cellulose, hemicellulose, and lignin are the biomass

components. DTG curve showed four distinct stages for weight loss. Between 50 °C and 150 °C, the initial weight loss happened. The hemicellulose degradation was responsible for the second stage, which occurred between 200 and 260 °C and had the highest rate of weight loss at 203 °C. The thermal breakdown of cellulose was represented by the third stage, which proceeded between 300 and 350 °C and had the largest weight loss percentage at 314 °C. The final stage of weight loss, linked to the lignin decomposition, revealed itself between 150 and 480 °C [41,42]. In the literature, it was extensively established that the various weight loss stages were associated with hemicellulose, cellulose, and lignin during the pyrolysis of other lignocellulosic compounds [37]. Thermal degradation caused 76.99 % weight loss of sugar beet pulp.

SEM images of SBP

Fig. S3a illustrated the SEM image of *SBP* at a magnification of 500x. Even though there were recess ledge fragments present, the SEM image revealed layered-like structures. The biomass's low specific surface area was caused by its non-porous nature. The details regarding the inorganic composition of *SBP* were provided by the EDX results (Fig. S3b). The biomass structure was heterogeneous; hence the results could differ. It was evident from the EDX data, expressed as in a percent by atom, that the main constituents of *SBP* were carbon (55.92 %) and oxygen (43.22 %). Furthermore, silicon (0.52 %), magnesium (0.23 %), and aluminum (0.11 %) were found in the structure. The main method used to determine the carbon content of biomass is elemental analysis. EDX, applied together with SEM analysis, allows the researcher to determine the elements present in the structure to receive details about the chemical composition. EDX is generally regarded as a semi-quantitative elemental analysis technique, therefore, there may be differences between the contents determined by elemental analysis and EDX analyses.

Catalyst Characterization

N_2 adsorption/desorption analysis

The usual Brunauer, Emmett, and Teller (BET) method was used to measure the surface areas (S_{BET}) of the metal-loaded catalysts. Table 2 listed the physicochemical characteristics of the catalytic materials utilized in the catalytic pyrolysis of *SBP*. As can be observed in Table 2, the largest surface area was obtained for Ni/Al_2O_3 (26.48 m^2/g), and the smallest was for Co/Al_2O_3 (11.72 m^2/g). It could be pointed out that with the existence of cobalt, a bigger pore size (95.87 nm) was obtained. The N_2 adsorption/desorption isotherms of the synthesized metal-loaded alumina catalysts indicated typical mesopore type IV hysteresis curves according to the isotherm types defined by IUPAC (Fig. 1). According to the IUPAC hysteresis loop classification, only the Ca/Al_2O_3 catalyst exhibited H3-type hysteresis, which appeared in materials with slit-shaped pores. In contrast, other catalysts displayed H2-type hysteresis, indicating materials are usually disordered where the pore size distribution and shape were not well defined, and also denoting bottleneck constrictions [43]. The pore sizes of metal-incorporated alumina catalysts (D_p) varied between 49 and 96 nm. With minimal textural and structural defects that contributed to the detected restricted micro- or *meso*-porosity, these pore diameters and the pore volume data (V_{total}) indicated that catalysts were extremely macroporous. This result

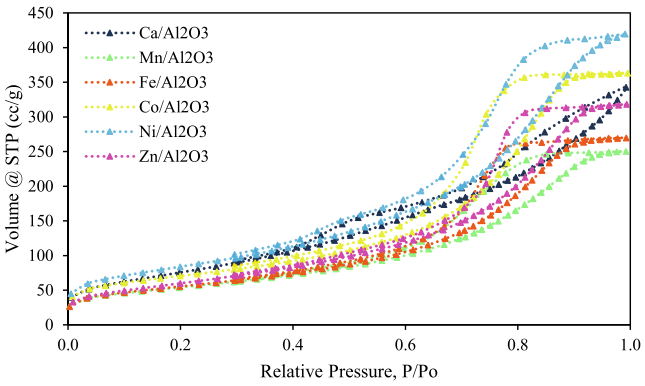

Fig. 1. N_2 adsorption/desorption isotherms of Me/Al_2O_3 catalysts.

was suitable with the literature [44].

X-ray diffraction analysis

The x-ray diffraction (XRD) technique is the most useful analytical method to examine the phase compositions and crystal structures of prepared catalytic materials. The x-ray diffraction patterns of the synthesized alumina-supported metal catalysts were demonstrated in Fig. 2, and the characteristic peaks corresponded to the standard card numbers issued by the Joint Committee on Powder Diffraction Standards (JCPDS). For the Ca/Al_2O_3 catalyst, the diffraction peaks at $2\theta = 39.43°$, 45.88°, and 66.85° were matched to cubic gamma-phase aluminum oxide (γ-Al_2O_3) (*JCPDS#98–003-0267*). In addition, peaks at $2\theta = 29.45°$ and 37.60° for Ca/Al_2O_3 catalyst were seen, which were attributed to the characteristic peaks of hexagonal Ca (*JCPDS#96–900-8490*) and cubic lime (CaO) (*JCPDS#96–900-6705*), respectively. Due to the XRD pattern of the Mn/Al_2O_3 catalyst, the peaks of parent cubic γ-Al_2O_3

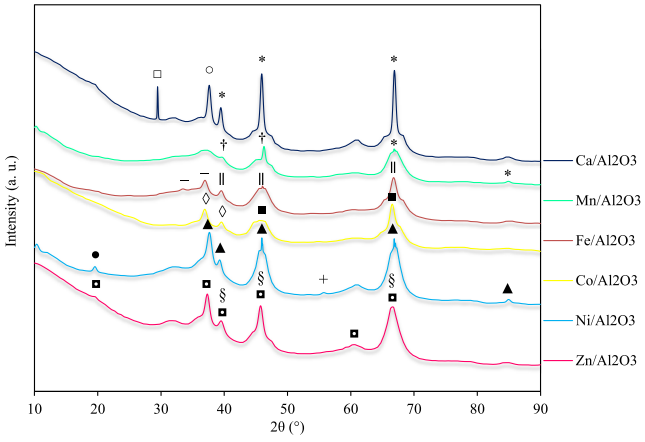

Fig. 2. XRD patterns of Me/Al_2O_3 catalysts (*: cubic γ-Al_2O_3, □: hexagonal Ca, ○: cubic CaO, †: γ-Al_2O_3-$Al_{57}Mn_{12}$, –: cubic α-Fe_2O_3, ‖: γ-Al_2O_3-Fe_2O_3, ◊:cubic Co_3O_4, ■:cubic γ-Al_2O_3-Co_3O_4, ●: cubic $NiAl_2O_4$, +: orthorhombic Al_2O_3, ▲: Al_2O_3-$NiAl_2O_4$, ◘:cubic Al_2O_3, §: cubic ZnO).

Table 2
Physical properties and EDX analysis results based on C atom (at.%) of metal-loaded alumina catalysts.

Catalyst type	S_{BET} (m^2/g)	D_p (nm)	V_{total} (cm^3/g)	*Elements, C Atom. (at.%)*							
				Al	O	Ca	Mn	Fe	Co	Ni	Zn
Ca/Al_2O_3	18.17	58.54	0.53	46.50	53.02	0.49	–	–	–	–	–
Mn/Al_2O_3	13.32	58.14	0.39	52.43	45.92	–	1.65	–	–	–	–
Fe/Al_2O_3	13.22	63.14	0.42	43.27	48.00	–	–	8.73	–	–	–
Co/Al_2O_3	11.72	95.87	0.56	35.27	63.84	–	–	–	0.89	–	–
Ni/Al_2O_3	26.48	49.00	0.65	37.36	61.71	–	–	–	–	0.93	–
Zn/Al_2O_3	14.57	49.21	0.68	39.79	59.24	–	–	–	–	–	0.98

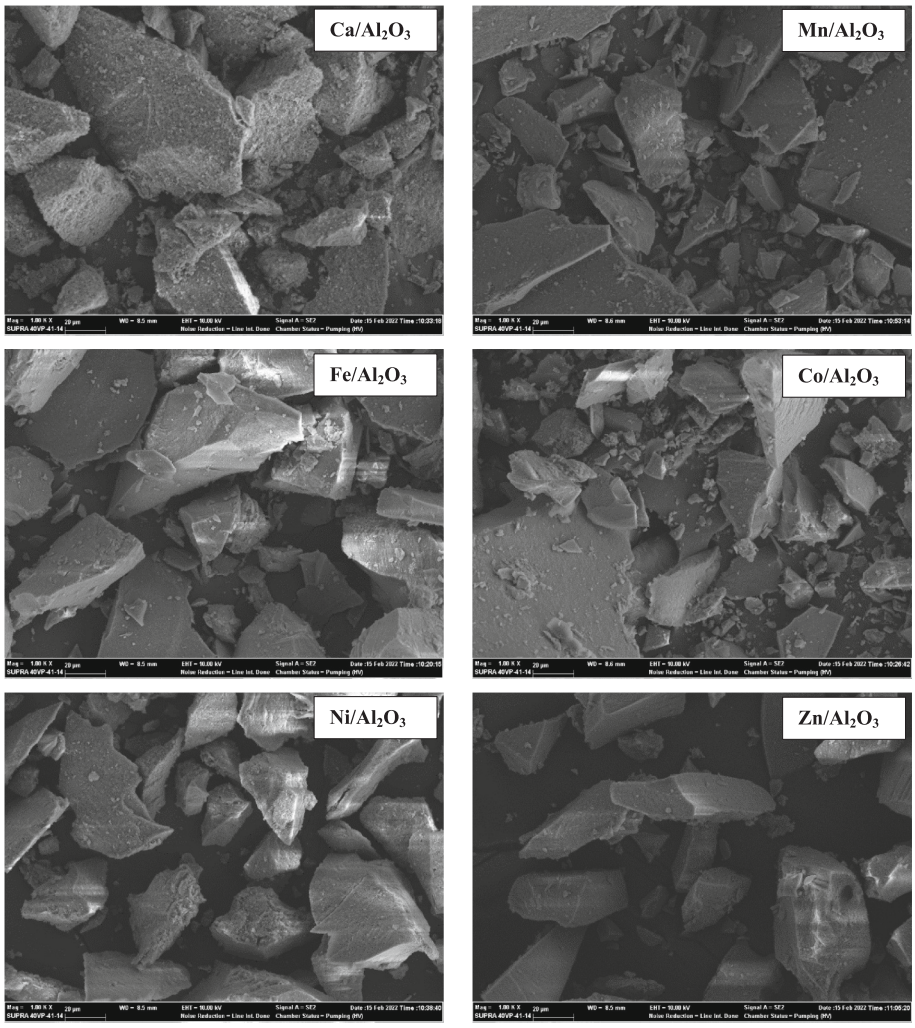

Fig. 3. SEM images of the alumina-supported metal catalysts.

were identified at 2θ = 66.85° and 84.85° (*JCPDS#98–003-0267*), and the cubic phase of aluminum manganese ($Al_{57}Mn_{12}$) was detected by the peak at 2θ = 10.22° (*JCPDS#98–001-4374*). The presence of the γ-Al_2O_3-$Al_{57}Mn_{12}$ structure was verified by the peaks at 2θ = 39.73° and 46.25°. However, no detectable MnO_x peaks were found in the Mn/Al_2O_3 structure, which could be attributed to the metal oxide's homogeneous dispersion [45,46]. Peaks at 2θ = 33.41° and 36.95° attributed to cubic α-Fe_2O_3 in the Fe/Al_2O_3 catalyst's XRD pattern (*JCPDS#98–010-8905*). The identification of the α-Fe_2O_3 phase suggested that a limited quantity of Fe^{3+} may integrate into the γ-Al_2O_3 crystal lattice. In addition, γ-Al_2O_3-Fe_2O_3 was identified by peaks found at 2θ = 39.52°, 46.03°, and 66.71° (*JCPDS#98–003-0267*) and the intensities of these peaks were higher than that of Fe_2O_3. Iron ions were dispersed throughout the catalyst surface during catalyst preparation, contributing to the γ-Al_2O_3-Fe_2O_3 structures' development. The x-ray diffraction pattern of the Co/Al_2O_3 catalyst characterized it by crystalline phases associated with Co_3O_4 and γ-Al_2O_3. The literature suggests that the Co_3O_4 of the spinel structure and the $CoAl_2O_4$ (cobalt aluminate) could be responsible for the diffraction peaks at 2θ = 32°, 37°, 45°, 60°, and 66° [47]. As given in Fig. 2, the peaks at 2θ = 36.90° and 39.54° attended the cubic phase spinel (Co_3O_4) structure (*JCPDS#98–017-3821*). Moreover, peaks obtained at 2θ = 44.57° and 66.49° with high intensities were attributed to the cubic phase of γ-Al_2O_3-Co_3O_4 (*JCPDS#98–003-0267, JCPDS#98–017-3821*), these peaks were more significant than that of spinel structure. The absence of any peaks containing just Al_2O_3 demonstrated that cobalt was dispersed over the catalyst surface. The diffraction peak at 2θ = 19.54° in the XRD pattern of the Ni/Al_2O_3 catalyst was assigned to a cubic phase nickel dialuminate ($NiAl_2O_4$) (*JCPDS#98–015-7690*) and the peak at 2θ = 55.65° was attended orthorhombic Al_2O_3 phase (*JCPDS#98–016-1061*). Other peaks at 2θ values of 37.64°, 39.28°, 45.94°, 66.87°, and 84.88° corresponded to the combination of orthorhombic Al_2O_3 and cubic $NiAl_2O_4$ structures. The lack of Ni and NiO peaks pointed out that nickel and nickel oxide had fully reacted with alumina into the nickel dialuminate phase. Moreover, the sharp peaks in the XRD pattern of the Ni/Al_2O_3 catalyst indicated high crystallinity and this result was in agreement with the literature [48–50]. As seen in the Zn/Al_2O_3 XRD pattern, peaks at 2θ = 19.57°, 37.30°, and 60.51° were matched with cubic Al_2O_3 phase (*JCPDS#96–153-1490*). Also, peaks observed at 2θ = 39.52°, 45.72°, and 66.55° denoted both Al_2O_3 (*JCPDS#96–153-1490*) and ZnO (*JCPDS#98–016-6358*) cubic phases. A limited quantity of Zn^{2+} could be integrated into the cubic Al_2O_3 crystal lattice, according to the zincite (ZnO) phase identification.

SEM analysis

SEM images of alumina-supported metal catalysts synthesized by the co-precipitation method were given at x1000 magnification in Fig. 3, and the EDX analysis results of all catalysts were listed in Table 2. As clearly seen from the SEM images, the metal dopants did not affect the morphological structure of all metal-loaded catalysts. On the other hand, the catalyst particles had angular morphologies with wide size ranges, and the metals were homogeneously dispersed on the alumina

surface, similar results were found in the literature [18,19].

FTIR spectra of the catalysts

The Fourier transform infrared (FTIR) spectrum of metal-loaded alumina catalysts can indicate valuable information about the surface properties, and chemical interactions occurring on the catalyst's surface. Examining the FTIR spectrum of metal-loaded alumina catalysts, several characteristic bands were observed:

i) Alumina bands: Alumina displayed distinct absorption bands, such as a broad band between 3600 and 3200 cm^{-1}, because of the stretching vibrations of hydroxyl groups (Al-OH), and provided details about the surface's hydrophilic properties. Around 1100–1000 cm^{-1}, connected to the Al-O stretching vibrations, was another significant band.
ii) Metal-oxygen bands: The presence of metal on the alumina catalyst could result in the observation of extra bands connected to the metal–oxygen vibrations. The specific metal present determined the location and strength of these bands.

As seen from the FTIR spectra of metal-loaded alumina catalysts in Fig. 4, broad absorption peaks were observed between 3410 and 3372 cm^{-1} for all catalysts belonging to hydroxyl groups on the alumina surface. The bands near 1445–1450 cm^{-1} and 1598 cm^{-1} were attributed to the –OH groups' bending vibration and the Al-O bonds' (Al-OH or Al-OH_2 groups) stretching vibration in alumina and were connected to Lewis acidity. These groups had the potential to function as acidic sites on the aluminum oxide surface and served as catalysts in a variety of chemical processes. Peaks showing Lewis acid parts were observed at approximately 1440 cm^{-1} for all alumina-supported metal-loaded catalysts. The peak intensities observed at 1440 cm^{-1} were obtained very close to each other in all catalysts. Me/Al_2O_3 catalysts showed characteristic vibrational peaks belonging to Me-O, Al-O, and Me-O-Al structures in the range of 900–450 cm^{-1} [51]. Peaks indicating Bronsted acidity were also observed at 1540 cm^{-1} and 1640 cm^{-1}. For Me/Al_2O_3 type catalysts, the band seen between 500–400 cm^{-1} revealed the presence of an Al-O bond, which is a commonly marked feature in metal oxides and can be seen in different shapes depending on the symmetry of the crystal structure and confirms the presence of the metal on the aluminum oxide surface [52].

The peaks around 660, 560, and 517 cm^{-1} for the Co/Al_2O_3 catalyst belonged to the Co-O-Al, Al-O, and Co-O vibrational modes. A weak peak between 670 cm^{-1} and 570 cm^{-1} indicated the presence of a Co_3O_4 structure and was seen when cobalt was in tetrahedral form. When the FTIR spectrum of the Ni/Al_2O_3 catalyst was examined, the weak absorption bands observed at 700 cm^{-1} as a shoulder and between 510–690 cm^{-1} belonged to Ni-O-Al, Al-O, and Ni-O stretching vibrations. Similarly, the bands noticed between 800–500 cm^{-1} for the Ca/Al_2O_3 catalyst, between 777–549 cm^{-1} for the Mn/Al_2O_3 catalyst, and between 808–513 cm^{-1} for the Zn/Al_2O_3 catalyst belong to Me-O-Al, Al-O, and Me-O (where Me: Ca, Mn and Zn) stretching vibrations in Fig. 4. In the Fe/Al_2O_3 catalyst's FTIR spectrum, the vibration peak at 446 cm^{-1} was associated with α-Fe_2O_3, and the peak at 570 cm^{-1} was the Al-O-Al peak of the γ-Al_2O_3 structure.

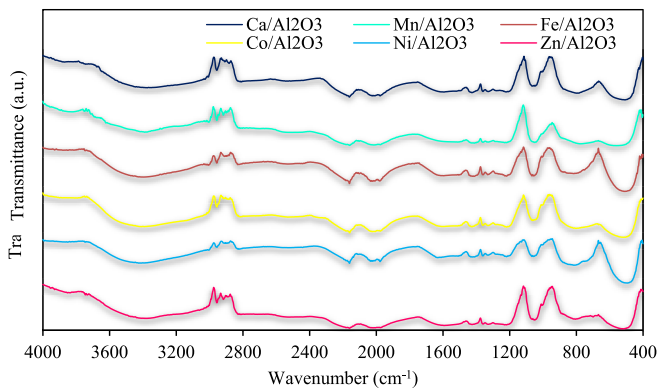

Fig. 4. FTIR spectrum of Me/Al_2O_3 catalysts.

Py-GC/MS analysis of SBP

Non-catalytic experiments

The qualitative composition data for the volatile sugar beet pulp components derived from non-catalytic Py-GC/MS analysis was shown in Fig. 5. The findings indicated that the sugar beet pulp pyrolysis produced a variety of organic compounds with carbon atoms ranging from C_5 to C_{31}. The pyrolytic products of sugar beet pulp were formed from the cellulose, hemicellulose, and lignin degradation. The majority of these products were aromatics, acids, hydrocarbons, alcohols, and ketones. However, the primary product was an acid that could be classified as undesirable since it increased the bio-oil corrosivity. Despite that, hydrocarbons, alcohols, ketones, and aromatics were desirable substances that could be employed to create beneficial components like fuels and aromatic compounds, among others. Bio-oil stability was reduced by aldehydes and ketones, which were reactive substances. However, ketones could also be employed to create functional compounds. Alcohols, phenols, aromatic hydrocarbons, and aliphatics were desirable in the liquid pyrolysis product. Although all of these ingredients were utilized to produce valuable chemicals, phenolic and aliphatic compounds were also used in fuel manufacturing. Using the chromatographic peak areas' percentage of non-catalytic Py-GC/MS experiments, a semi-quantitative analysis was conducted to ascertain the volatile components' distribution. The peak area of the aromatic compounds was 24.14 %, as shown in Fig. 5. In terms of acids, alcohols, ketones, hydrocarbons, and aldehydes, the peak areas of various other chemical substances were found to be 24.53 %, 20.09 %, 17.68 %, 3.01 %, and 6.96 %, respectively. Catalytic pyrolysis could reduce unwanted product yield and enhance desired component yield by loading catalysts with transition metals (Mn, Fe, Co, Ni, and Zn) or alkaline earth metals (i.e., Ca).

Catalytic experiments utilizing Me/Al_2O_3 catalysts

Pyrolysis is a complicated process because various variables affect the chemical composition of the bio-oil. The type of catalyst and temperature are two key operating parameters in the pyrolysis process that have a significant impact on the final product's distribution and quality. Typically, a catalyst is essential to the pyrolysis process because it breaks down the sugar derivatives from the pyrolysis of both hemicellulose and cellulose fractions into lighter alcohols, ketones, and furans through the reactions of decarbonylation, dehydration, decarboxylation, and

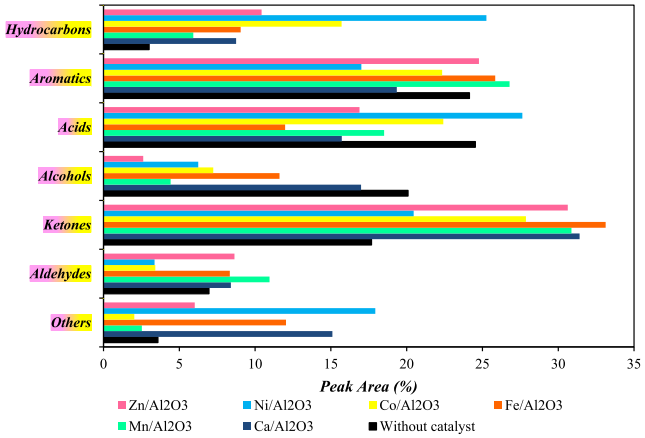

Fig. 5. Chemical composition of non-catalytic and catalytic pyrolysis products.

cracking, which then result in the conversion of them into phenols and hydrocarbons [20]. Employing metal-supported or metal oxide catalysts restricts the production of carboxylic acids and oxygenated compounds while boosting the output of hydrocarbons, hence minimizing the bio-oil's corrosiveness, water, and oxygen contents [53]. To lessen the amount of undesired products of the sugar beet pulp pyrolysis, catalytic Py-GC/MS studies were conducted in the presence of Me/Al_2O_3 (Me: Ca, Mn, Fe, Co, Ni, and Zn) catalysts (Fig. 5). Additionally, it aimed to boost the output of valuable chemicals such as aromatics and hydrocarbons, which were the desired compounds. The catalyst that increased the -hydrocarbons was found to be the most acceptable when comparing the effect of metal-incorporated alumina catalysts on pyrolysis products. Ni/Al_2O_3 catalyst yielded a peak area of the greatest hydrocarbon content of 25.26 %. This result was consistent with the information in the literature and supported that metal-incorporated catalysts enhance deoxygenation activity by increasing hydrocarbon yield [54,55]. When the amount of the acidic compounds obtained in catalytic pyrolysis reactions were compared, catalysts loaded with Mn, Ca, Zn, and Fe significantly changed the amount of acid in the volatiles and the lowest peak area at 11.98 % was obtained in acidic compounds with the Fe-loaded catalyst. The integration of metal-loaded catalysts in the pyrolysis reaction caused hydrogenation reactions that altered the chemical composition of bio-oil [56]. Carboxylic acids undertake a ketonization reaction, which eliminates CO_2 and H_2O before achieving C–C coupling by aldol condensation, resulting in enhanced carbon chain length [57]. Another important source of chemical raw materials was product-by-product aromatic compounds. The improved yields of these compounds were achieved by implementing Mn, Fe, and Zn catalysts, respectively, because pyrolysis vapors allowed these smaller molecules to enter due to the breakdown of heavy molecules. Catalysts can facilitate the interactive transformations (i.e. isomerization, trans alkylation, and polymerization) of mono-phenolic compounds formed by lignin decomposition, the interaction of olefins with low molecular weight oxygenates (such as furans, ketones, and alcohols), and formation of a variety of aromatic compounds by further dehydration of phenolics [20]. The amount of aromatic hydrocarbons could be raised by increasing the porosity of the catalyst and catalyzing aromatization reactions. Upgrading the biomass pyrolysis vapor with a peroxidation catalyst allows for the linear conversion of alcohol to aldehydes, acids, and ketones [58]. Also, the decrease in the portion of alcohols and acids among the volatile products of catalytic pyrolysis was associated with the transformation of alcohols into aldehydes and ketones as a result of the oxidation reaction [58,59].

The schematic diagram of the main catalytic pyrolysis reaction mechanisms for lignocellulosic biomass with Me/Al_2O_3 catalysts was displayed in Fig. 6. When the effects of Me/Al_2O_3 catalysts used in this study on the catalytic pyrolysis of *SBP* were examined, it was clear that all catalysts enabled the conversion of alcohols to ketones or aldehydes. The increase in the proportion of ketones among the pyrolysis volatile components for all catalysts was due to the conversion of alcohols or acids into ketones. Accordingly, the decrease in the portion of acidic components (except for the Ni/Al_2O_3 catalyst) supported the formation of ketones as a result of the ketonization reaction, and the decline in the part of alcohols (except for the Ni and Co-loaded alumina catalysts) conducted the formation of aldehydes and ketones by oxidation reactions. It could be concluded that during the degradation of cellulose with the Ni/Al_2O_3 catalyst, more carboxylic acid compounds were formed; a small part of them turned into ketone, and the rest did not react. This could also be supported by the fact that the lowest aldehydes ratio was obtained using the nickel-loaded catalyst compared to other Me/Al_2O_3 catalysts. In addition, the Ni/Al_2O_3 catalyst restricted the formation of aromatic compounds by preventing cracking and aromatization reactions. The Co/Al_2O_3 catalyst enabled the conversion of acids and alcohols to ketones via ketonization and oxidation reactions, respectively, but limited the conversion of alcohols to aldehydes via

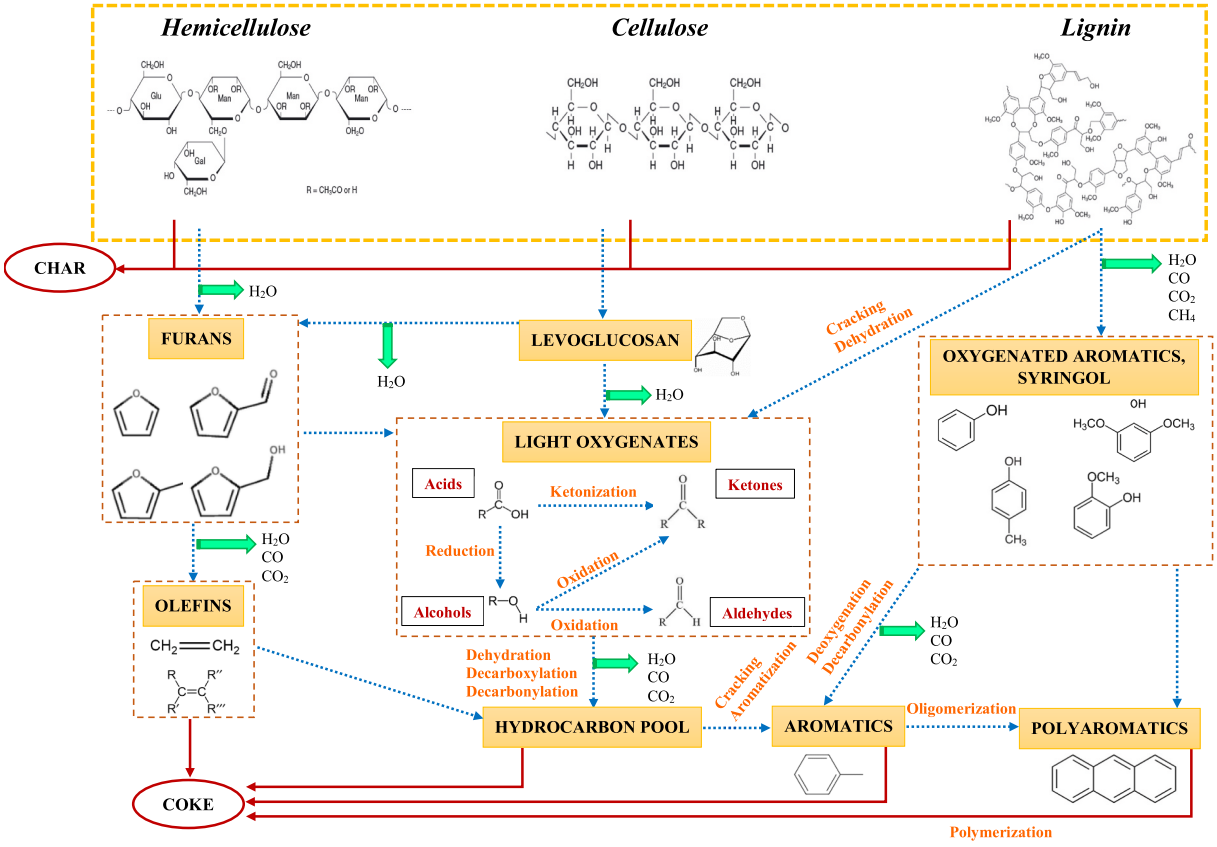

Fig. 6. The schematic diagram of the main catalytic pyrolysis reaction mechanisms for lignocellulosic biomass with Me/Al_2O_3 catalysts (adapted from [7,60–62]).

oxidation reaction. Similar to the Ni/Al_2O_3 catalyst, alumina catalysts loaded with both Co and Ca metals promoted the conversion of light oxygenates to hydrocarbons, while inhibiting the conversion of HCs to aromatics via cracking and aromatization reactions. Alumina catalysts loaded with Zn, Mn, and Ca metals led to the conversion of both acids and alcohols to ketones and aldehydes; low molecular weight oxygenates derived from hemicellulose, cellulose, and lignin structures produced HCs by dehydration, decarboxylation, and decarbonylation reactions; and directed the formation of aromatics by their oligomerization. Besides, the formation of phenolic compounds instead of light oxygenates as a result of the degradation of lignin in the biomass structure through cracking and dehydration reactions under the influence of Zn-, Mn-, and Ca-loaded Al_2O_3 catalysts and the conversion of these oxygenated aromatics into aromatics by deoxygenation and decarbonylation reactions could be explained by the low HCs content in the volatile product distribution. In summary, when the effects of all catalysts on the pyrolysis product distribution were examined, it was determined that Ni/Al_2O_3 and then Co/Al_2O_3 catalysts were most significant in obtaining hydrocarbons, one of the valuable compounds, with the highest conversion, and Mn/Al_2O_3 and Fe/Al_2O_3 catalysts were important in producing aromatics, the second most valuable compound group.

Conclusion

The development of renewable biofuels is gaining a lot of attention due to their ecologically friendly nature and potential to provide a longer-term, more sustainable solution to the world's energy demands. Sugar beet pulp from sugar factory waste is a crucial biomass source for Turkey and many other countries, as it is abundant and cheap. In recent years, the usage of factory waste in energy production has become rapidly widespread. The current concerns of the economy, environment, and energy all required to be handled concurrently; in particular, the economy, environment, and society all depended heavily on a consistent, affordable, and clean supply of energy and resources. In this study conducted for this purpose, it was revealed that sugar beet pulp could be evaluated both as a chemical raw material source and as liquid fuel by catalytic and non-catalytic Py-GC/MS methods. Catalysts used in catalytic pyrolysis are composite structures consisting of support and active parts. While the support material improves properties such as surface area and thermal stability, the added metals act as the active phase and affect the product yield and selectivity according to the relevant reaction. Even if the catalyst's surface area is low, the reaction is shaped depending on the type of selected active metal, and the product distribution varies. In addition to being cost-effective, alumina-supported catalysts exhibit high activity owing to their acidic nature, excellent water absorption capabilities, and cracking reaction success. Considering that metal-incorporated catalysts are highly active in the deoxygenation and dehydration reactions, the selectivity of the product could be increased by synthesizing suitable catalysts and using them in pyrolysis reactions, so the additional cost and energy needs could be reduced.

CRediT authorship contribution statement

Nurgül Özbay: Writing – original draft, Supervision, Methodology, Conceptualization. **Adife Şeyda Yargıç:** Writing – review & editing, Visualization, Investigation, Formal analysis. **Aydan Tatman:** Formal analysis. **Fatma Eroğlu:** Supervision.

Declaration of competing interest

The authors declare that they have no known competing financial interests or personal relationships that could have appeared to influence the work reported in this paper.

Appendix A. Supplementary data

Supplementary data to this article can be found online at https://doi.org/10.1016/j.seta.2025.104323.

Data availability

The authors do not have permission to share data.

References

[1] Ly HV, Park JW, Kim SS, Hwang HT, Kim J, Woo HC. Catalytic pyrolysis of bamboo in a bubbling fluidized-bed reactor with two different catalysts: HZSM-5 and red mud for upgrading bio-oil. *Renew Energy* 2020;149:1434–45.

[2] Qiu B, Tao X, Wang J, Liu Y, Li S, Chu H. Research progress in the preparation of high-quality liquid fuels and chemicals by catalytic pyrolysis of biomass: A review. *Energ Conver Manage* 2022;261:115647.

[3] Liu R, Sarker M, Rahman MM, Li C, Chai M, Cotillon R, et al. Multi-scale complexities of solid acid catalysts in the catalytic fast pyrolysis of biomass for bio-oil production–A review. *Prog Energy Combust Sci* 2020;80:100852.

[4] Chen X, Che Q, Li S, Liu Z, Yang H, Chen Y, et al. Recent developments in lignocellulosic biomass catalytic fast pyrolysis: Strategies for the optimization of bio-oil quality and yield. *Fuel Process Technol* 2019;196:106180.

[5] Duan Y, Pandey A, Zhang Z, Awasthi MK, Bhatia SK, Taherzadeh MJ. Organic solid waste biorefinery: Sustainable strategy for emerging circular bioeconomy in China. *Ind Crop Prod* 2020;153:112568.

[6] Sharifzadeh M, Sadeqzadeh M, Guo M, Borhani TN, Konda NM, Garcia MC, et al. The multi-scale challenges of biomass fast pyrolysis and bio-oil upgrading: Review of the state of art and future research directions. *Prog Energy Combust Sci* 2019;71:1–80.

[7] Wang Y, Akbarzadeh A, Chong L, Du J, Tahir N, Awasthi MK. Catalytic pyrolysis of lignocellulosic biomass for bio-oil production: A review. *Chemosphere* 2022;297:134181.

[8] Wang J, Xu C, Zhong Z, Deng A, Hao N, Li M, Meng X, Ragauskas AJ. Catalytic Conversion of Bamboo sawdust over ZrO_2–CeO_2/γ-Al_2O_3 to produce ketonic hydrocarbon precursors and furans. ACS Sustain Chem Eng 2018;6(11):13797–806.

[9] Dai L, Wang Y, Liu Y, He C, Ruan R, Yu Z, et al. A review on selective production of value-added chemicals via catalytic pyrolysis of lignocellulosic biomass. *Sci Total Environ* 2020;749:142386.

[10] Farahmandjou M, Khodadadi A, Yaghoubi M. Low Concentration Iron-Doped Alumina (Fe/Al_2O_3) Nanoparticles Using Co-Precipitation Method. *J Supercond Nov Magn* 2020;33:3425–32.

[11] Turkish Sugar Company (TürkŞeker) 2020. Agricultural Products Markets Sugar Report.

[12] Bensidhom G, Arabiourrutia M, Trabelsi ABH, Cortazar M, Ceylan S, Olazar M. Fast pyrolysis of date palm biomass using Py-GCMS. *J Energy Inst* 2021;99:229–39.

[13] Ozbay N, Yargic AS, Sahin RZY. Tailoring Cu/Al_2O_3 catalysts for the catalytic pyrolysis of tomato waste. *J Energy Inst* 2018;91(3):424–33.

[14] Iliopoulou EF, Stefanidis SD, Kalogiannis KG, Delimitis A, Lappas AA, Triantafyllidis KS. Catalytic upgrading of biomass pyrolysis vapors using transition metal-modified ZSM-5 zeolite. *Appl Catal B* 2012;127:281–90.

[15] de Medeiros AM, de Sousa Castro K, de Macêdo MLG, de Morais Araújo AM, da Silva DR, Gondim AD. Catalytic pyrolysis of coconut oil with Ni/SBA-15 for the production of bio jet fuel. *RSC Adv* 2022;12(16):10163–76.

[16] Widyaningrum RN, Church TL, Zhao M, Harris AT. Mesocellular-foam-silica-supported Ni catalyst: Effect of pore size on H_2 production from cellulose pyrolysis. *Int J Hydrogen Energy* 2012;37(12):9590–601.

[17] Zheng Y, Wang F, Yang X, Huang Y, Liu C, Zheng Z, et al. Study on aromatics production via the catalytic pyrolysis vapor upgrading of biomass using metal-loaded modified H-ZSM-5. *J Anal Appl Pyrol* 2017;126:169–79.

[18] Özbay N, Yargıç AŞ, Şahin RZY, Yaman E. Research on the Pyrolysis Characteristics of Tomato Waste with Fe–Al_2O_3 Catalyst. In: *Exergetic, Energetic and Environmental Dimensions*. Academic Press; 2018. p. 815–28.

[19] Tatman A, Yargıç AŞ, Özbay N, Eroğlu F. Synthesis of Fe/Al_2O_3 Catalyst Using Co-Precipitation Method and its Use in Py-Gc/Ms System. BZT Academy Publishing House; 2022.

[20] Singh R, Chakinala N, Mohanty K, Chakinala AG. Catalytic upgrading of biomass pyrolysis vapors for selective production of phenolic monomers over metal oxide modified alumina catalysts. *J Environ Chem Eng* 2023;11(6):111518.

[21] Choi YS, Choi SK, Kim SJ, et al. Fast pyrolysis of coffee ground in a tilted-slide reactor and characteristics of biocrude oil. *Environ Prog Sustain Energy* 2017;36(3):655–61.

[22] Muley PD, Henkel C, Abdollahi KK, Marculescu C, Boldor D. A critical comparison of pyrolysis of cellulose, lignin, and pine sawdust using an induction heating reactor. *Energ Conver Manage* 2016;117:273–80.

[23] Williams PT, Nugranad N. Comparison of products from the pyrolysis and catalytic pyrolysis of rice husks. *Energy* 2000;25(6):493–513.

[24] Zhao N, Li BX. The effect of sodium chloride on the pyrolysis of rice husk. *Appl Energy* 2016;178:346–52.

[25] Pütün AE, Önal E, Uzun BB, Özbay N. Comparison between the "slow" and "fast" pyrolysis of tobacco residue. *Ind Crop Prod* 2007;26(3):307–14.

[26] Uzun BB, Pütün AE, Pütün E. Fast pyrolysis of soybean cake: Product yields and compositions. *Bioresour Technol* 2006;97(4):569–76.
[27] Demiral İ, Ayan EA. Pyrolysis of grape bagasse: effect of pyrolysis conditions on the product yields and characterization of the liquid product. *Bioresour Technol* 2011;102(4):3946–51.
[28] Apaydin-Varol E, Pütün E, Pütün AE. Slow pyrolysis of pistachio shell. *Fuel* 2007;86(12–13):1892–9.
[29] Pütün E. Catalytic pyrolysis of biomass: Effects of pyrolysis temperature, sweeping gas flow rate and MgO catalyst. *Energy* 2010;35(7):2761–6.
[30] Pütün E, Uzun BB, Pütün AE. Fixed-bed catalytic pyrolysis of cotton-seed cake: effects of pyrolysis temperature, natural zeolite content and sweeping gas flow rate. *Bioresour Technol* 2006;97(5):701–10.
[31] Yaman E. Influence of catalyst support type on silver poplar pyrolysis vapors: a Py/GC-MS study. *J Porous Mater* 2023;30(5):1427–38.
[32] Jeon MJ, Jeon JK, Suh DJ, Park SH, Sa YJ, Joo SH, et al. Catalytic pyrolysis of biomass components over mesoporous catalysts using Py-GC/MS. *Catal Today* 2013;204:170–8.
[33] Lu Q, Zhou MX, Li WT, Wang X, Cui MS, Yang YP. Catalytic fast pyrolysis of biomass with noble metal-like catalysts to produce high-grade bio-oil: analytical Py-GC/MS study. *Catal Today* 2018;302:169–79.
[34] Vichaphund S, Aht-ong D, Sricharoenchaikul V, Atong D. Catalytic upgrading pyrolysis vapors of Jatropha waste using metal promoted ZSM-5 catalysts: an analytical PY-GC/MS. *Renew Energy* 2014;65:70–7.
[35] Zhang B, Zhong Z, Ding K, Song Z. Production of aromatic hydrocarbons from catalytic co-pyrolysis of biomass and high density polyethylene: analytical Py–GC/MS study. *Fuel* 2015;139:622–8.
[36] Muzyka R, Sobek S, Dudziak M, Ouadi M, Sajdak M. A comparative analysis of waste biomass pyrolysis in Py-GC-MS and fixed-bed reactors. Energies 2023;16(8):3528.
[37] Özbay N, Pütün AE. Characterization of chars from steam pyrolysis of apricot pulp. *Energy Sources Part A* 2011;33(16):1504–13.
[38] Gómez-Serrano V, Piriz-Almeida F, Durán-Valle CJ, Pastor-Villegas J. Formation of oxygen structures by air activation. A study by FT-IR spectroscopy. *Carbon* 1999;37(10):1517–28.
[39] Gómez-Serrano V, Pastor-Villegas J, Perez-Florindo A, Duran-Valle C, Valenzuela-Calahorro C. FT-IR study of rockrose and of char and activated carbon. *J Anal Appl Pyrol* 1996;36(1):71–80.
[40] Özbay N, Uzun BB, Varol EA, Pütün AE. Comparative analysis of pyrolysis oils and its subfractions under different atmospheric conditions. *Fuel Process Technol* 2006;87(11):1013–9.
[41] Apaydın Varol E, Mutlu Ü. TGA-FTIR analysis of biomass samples based on the thermal decomposition behavior of hemicellulose, cellulose, and lignin. *Energies* 2023;16(9):3674.
[42] Kiełbasa K, Bayar Ş, Varol EA, Sreńscek-Nazzal J, Bosacka M, Michalkiewicz B. Thermochemical conversion of lignocellulosic biomass-olive pomace-into activated biocarbon for CO_2 adsorption. *Ind Crop Prod* 2022;187:115416.
[43] ALOthman ZA. A review: fundamental aspects of silicate mesoporous materials. *Materials* 2012;5(12):2874–902.
[44] Shafiee P, Alavi SM, Rezaei M. Investigation of the effect of cobalt on the Ni–Al_2O_3 catalyst prepared by the mechanochemical method for CO_2 methanation. *Res Chem Intermed* 2022;48(5):1923–38.
[45] Filipović S, Obradović N, Marković S, Djordjević A, Balac I, Dapcević A, et al. Physical properties of sintered alumina doped with different oxides. *Sci Sinter* 2018;50(4):409–19.
[46] Ryu HW, Song MY, Park JS, Kim JM, Jung SC, Song J, et al. Removal of toluene using ozone at room temperature over mesoporous Mn/Al_2O_3 catalysts. *Environ Res* 2019;172:649–57.
[47] Nuernberg GB, Fajardo HV, Mezalira DZ, Casarin TJ, Probst LF, Carreño NL. Preparation and evaluation of Co/Al_2O_3 catalysts in the production of hydrogen from thermo-catalytic decomposition of methane: Influence of operating conditions on catalyst performance. *Fuel* 2008;87(8–9):1698–704.
[48] He L, Ren Y, Yue B, Tsang SCE, He H. Tuning metal–support interactions on Ni/Al_2O_3 catalysts to improve catalytic activity and stability for dry reforming of methane. *Processes* 2021;9(4):706.
[49] Ragupathi C, Vijaya JJ, Kennedy LJ. Preparation, characterization and catalytic properties of nickel aluminate nanoparticles: A comparison between conventional and microwave method. *J Saudi Chem Soc* 2017;21:S231–9.
[50] Zygmuntowicz J, Wiecińska P, Miazga A, Konopka K. Characterization of composites containing $NiAl_2O_4$ spinel phase from Al_2O_3/NiO and Al_2O_3/Ni systems. *J Therm Anal Calorim* 2016;125:1079–86.
[51] Jiang Z, Zheng Z, Wu J, Liu X, Yu H, Shen J. Synthesis, characterization and performance of microorganism-embedded biocomposites of LDH-modified PVA/SA hydrogel beads for enhanced biological nitrogen removal process. *Process Biochem* 2022;121:542–52.
[52] Gonçalves AA, Costa MJ, Zhang L, Ciesielczyk F, Jaroniec M. One-pot synthesis of $MeAl_2O_4$ (Me= Ni, Co, or Cu) supported on γ-Al_2O_3 with ultralarge mesopores: enhancing interfacial defects in γ-Al_2O_3 to facilitate the formation of spinel structures at lower temperatures. *Chem Mater* 2018;30(2):436–46.
[53] Bhoi PR, Ouedraogo AS, Soloiu V, Quirino R. Recent advances on catalysts for improving hydrocarbon compounds in bio-oil of biomass catalytic pyrolysis. *Renew Sustain Energy Rev* 2020;121:109676.
[54] Aravind SV, Ahmed G, Kishore N. Pyrolysis of Delonix regia using metal oxide catalysts and solvent effect on fuel fraction of bio-oil. *Results Eng* 2023;17:100876.
[55] Li Y, Yellezuome D, Li C, Liu R. Deactivation mechanism and regeneration effect of bi-metallic Fe-Ni/ZSM-5 catalyst during biomass catalytic pyrolysis. *Fuel* 2022;312:122924.
[56] Wang H, Lee SJ, Olarte MV, Zacher AH. Bio-oil stabilization by hydrogenation over reduced metal catalysts at low temperatures. *ACS Sustain Chem Eng* 2016;4(10):5533–45.
[57] Pham TN, Shi D, Resasco DE. Evaluating strategies for catalytic upgrading of pyrolysis oil in liquid phase. *Appl Catal B* 2014;145:10–23.
[58] Shao S, Liu C, Xiang X, Li X, Zhang H, Xiao R. Insight into the selective production of aldehydes and ketones by catalytic upgrading of biomass pyrolysis vapor over ZrO2: Cellulose and xylan. *Biomass Bioenergy* 2022;162:106473.
[59] Kumar R, Enjamuri N, Shah S, Al-Fatesh AS, Bravo-Suarez JJ, Chowdhury B. Ketonization of oxygenated hydrocarbons on metal oxide based catalysts. *Catal Today* 2018;302:16–49.
[60] Khosravanipour Mostafazadeh A, Solomatnikova O, Drogui P, Tyagi RD. A review of recent research and developments in fast pyrolysis and bio-oil upgrading. *Biomass Convers Biorefin* 2018;8:739–73.
[61] Rangel MDC, Mayer FM, Carvalho MDS, Saboia G, de Andrade AM. Selecting catalysts for pyrolysis of lignocellulosic biomass. *Biomass* 2023;3(1):31–63.
[62] Ratnasari DK, Bijl A, Yang W, Jönsson PG. Effect of H-ZSM-5 and Al-MCM-41 proportions in catalyst mixtures on the composition of bio-oil in ex-situ catalytic pyrolysis of lignocellulose biomass. *Catalysts* 2020;10(8):868.